

CONFIDENTIAL

18230
18383
1957

Copy
RM L57

SEP 5

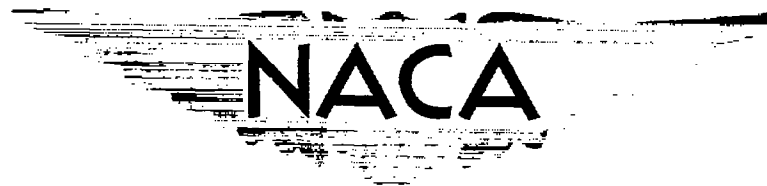
0144803



TECH LIBRARY KAFB, NM

NACA RM L57G30

7800



RESEARCH MEMORANDUM

FREE-FLIGHT SKIN-TEMPERATURE
AND SURFACE-PRESSURE MEASUREMENTS ON A HIGHLY POLISHED
NOSE HAVING A 100° TOTAL-ANGLE CONE AND A
 10° HALF-ANGLE CONICAL FLARE SECTION

UP TO A MACH NUMBER OF 4.08

By Bernard Rashis and Aleck C. Bond

Langley Aeronautical Laboratory
Langley Field, Va.

CLASSIFIED DOCUMENT

This material contains information affecting the National Defense of the United States within the meaning of the espionage laws, Title 18, U.S.C., Secs. 793 and 794, the transmission or revelation of which in any manner to an unauthorized person is prohibited by law.

**NATIONAL ADVISORY COMMITTEE
FOR AERONAUTICS**

WASHINGTON

August 23, 1957

CONFIDENTIAL



NATIONAL ADVISORY COMMITTEE FOR AERONAUTICS

RESEARCH MEMORANDUM

FREE-FLIGHT SKIN-TEMPERATURE
AND SURFACE-PRESSURE MEASUREMENTS ON A HIGHLY POLISHED
NOSE HAVING A 100° TOTAL-ANGLE CONE AND A
 10° HALF-ANGLE CONICAL FLARE SECTION
UP TO A MACH NUMBER OF 4.08

By Bernard Rashis and Aleck C. Bond

SUMMARY

The skin temperature and surface pressure have been measured on a large-scale, highly polished nose having a relatively sharp-tipped 100° total-angle cone followed by a conical flare section of 10° half-angle. The measurements were obtained in flight from a rocket-propelled model up to a peak Mach number of 4.08 and a peak Reynolds number of 22×10^6 per foot. Temperature distributions indicated that the heating on the forward 3.5 inches of the 100° cone was lower than the heating on the rearward portion. Likewise, measured temperatures on the flare portion of the test nose were generally lower than the temperatures on the 100° cone portion. The data indicated that the local Reynolds numbers of transition, based on calculated boundary-layer momentum thicknesses, ranged from 530 to 940 for a Mach number range from 2.72 to 3.75. Comparison of measured cone pressures with theory for a sharp cone showed that theory overestimates the cone pressures. Pressure measurements on the flare portion of the nose showed that in the lower speed range the flow expands below atmospheric pressure in going from the cone to the flare; however, as the speed increased, the expansion diminished and for speeds greater than a Mach number of approximately 3.0 the flare pressure coefficients were at or near a value of zero.

INTRODUCTION

A program for the investigation of aerodynamic heat transfer and boundary-layer transition on bodies in free flight at supersonic and hypersonic speeds is being conducted by the Langley Pilotless Aircraft

~~CONFIDENTIAL~~

Research Division. Several flight tests for the investigation of the heat transfer to conical noses of 10° to 25° total cone angle have been conducted and the results are reported in references 1, 2, and 3. The results of investigations on the heating and boundary-layer transition on large-scale conical noses of 29° and 50° total cone angle, including the effects of large bluntness, are reported in references 4 and 5, respectively.

The purpose of the present test was to extend the investigation to a conical nose of even larger total cone angle. The model employed in the test was a large-scale, relatively sharp, 100° total-angle conical nose followed by a 10° half-angle conical flare section. The flight test was conducted at the Langley Pilotless Aircraft Research Station at Wallops Island, Va. Heating data were obtained in the Mach number range from 1.74 to 4.08 corresponding to a free-stream Reynolds number range per foot of 6×10^6 to 22×10^6 , respectively.

SYMBOLS

C_p	pressure coefficient, $\frac{p - p_o}{q}$
M	Mach number
N_{St}	Stanton number
p	pressure, lb/sq in.
q	free-stream dynamic pressure, lb/sq ft
R	Reynolds number
T	temperature
t	time, sec
Subscripts:	
w	wall
∞	conditions outside boundary layer
o	free-stream conditions

- 1,2,3 pressure-measurement stations (see fig. 3)
0 momentum thickness

MODEL AND INSTRUMENTATION

The configuration of the actual test nose was a relatively sharp-tipped 100° total-angle cone with a 12-inch base diameter followed by a 3-inch-long conical flare section of 10° half-angle. The 10° half-angle conical flare section was continued rearward, however, until its diameter matched the 16.8-inch diameter of the M5 JATO rocket motor to which it was permanently affixed. The space within this transition section was utilized to house the telemeter. Figure 1 is a sketch showing pertinent construction details and dimensions of the test nose, and figure 2 shows a closeup photograph of the nose. The nominal thickness of the Inconel skin after spinning and light polishing was 0.029 inch. The surface roughness as measured by an interference microscope was of the order of 2 microinches. In order to minimize deformation of the thin skin material by the high-pressure loads, a magnesium innercone with a wall thickness of approximately 1 inch was used to support the test nose as shown in figure 1(b). Thermal insulation between the Inconel skin and the magnesium innercone was provided by a layer of balsa wood approximately $5/16$ inch thick.

The model was equipped with a telemetering system which transmitted nose skin temperatures, nose pressures, and thrust and drag accelerations to a ground receiving station during the flight. Twelve thermocouples were installed on the skin of the test nose at the locations indicated in figure 3(a). Thermocouples 1 to 9 were located along one meridian of the test nose, whereas thermocouples 10, 11, and 12 were spaced 90° apart on the 100° cone at the same longitudinal location as thermocouple 4. During the flight, thermocouple 10 failed to operate properly and will hence be excluded from the data presentation. The thermocouples were made of No. 30 chromel-alumel wire and were spot-welded to the inner surface of the Inconel skin. At the point where a thermocouple was attached to the skin, a clearance hole of approximately $1/4$ -inch diameter was cut in the balsa insulation in an attempt to minimize any local heat loss to the insulation. A check on the telemetered skin temperature was made just prior to launching by determining the temperature at one of the measurement stations of a thermocouple taped to the exterior surface of the skin.

During flight, three standard voltages and the outputs of six thermocouples were commutated on each of two telemeter channels so that the temperature of each station was recorded approximately every 0.1 second. The three standard voltages were chosen to be equivalent to the lowest,

middle, and highest temperatures that the skin was expected to reach. Commutation of the known voltages along with the thermocouple outputs provided an inflight check calibration of the temperature-measuring system.

Continuous pressure measurements were made on the test nose at the six locations shown in figure 3(b). The pressure orifices which were drilled with a No. 52 drill (0.0635 inch) were spaced along a meridian which was 45° from the meridian on which the line of thermocouples was located.

Other instrumentation consisted of ground-based radar units for measuring model velocity and for obtaining the position of the model in space. Velocity data were obtained by means of CW Doppler radar. An NACA modified SCR-584 tracking radar provided slant range, azimuth, and elevation angle from which the altitude, horizontal range, and model flight-path angle were determined. Integration of the telemetered thrust and drag acceleration provided a check on the Doppler radar velocity measurements. Atmospheric data and wind conditions were measured by means of a radiosonde launched near the time of flight and were tracked by a Rawin set AN/GMD-1A.

PROCEDURE

The model was ground launched at an elevation angle of 60° . A photograph of the model and boosters on the launcher is shown in figure 4. The first-stage booster was an M6 JATO rocket motor, and the second-stage booster to which the test nose was permanently mounted was an M5 JATO rocket motor.

The first stage or M6 JATO rocket motor has a nominal burning time of about 5 seconds. The electrical ignition squibs in the second-stage motor were selected with a delay time so that ignition would take place slightly after burnout of the first-stage motor; however, for reasons unknown, there was a premature firing of the second-stage motor about 3.25 seconds after take-off. The separation of the two rocket motors was clean and there was no damage to the second stage; however, it is estimated that there was a loss of about 0.7 in Mach number because of the premature ignition. The second-stage motor accelerated to a peak Mach number of 4.08 at about 6.5 seconds. Time histories of the free-stream Mach number and free-stream Reynolds number per foot of the flight test are shown in figure 5. The variation of the model flight velocity along with the altitude and corresponding free-stream density are shown as a function of time in figure 6. Figure 7 presents the variation of the free-stream static temperature, as determined by the

~~CONFIDENTIAL~~

radiosonde measurements, and the computed variation of the stream stagnation temperature corresponding to the Mach number time history shown in figure 5. The stagnation temperature was determined by taking into account the variation in the air specific heat in going from static temperature to total temperature.

During the firing of the second-stage rocket motor, commutation of the thermocouple pickups stopped, apparently as a result of the high longitudinal accelerations on the electric switching motor. For this reason, temperature data were not obtained on the test nose during the period between 3.25 and 6.7 seconds. The other instruments were unaffected by the acceleration, and continuous data were obtained all through the test.

TEMPERATURE MEASUREMENTS

Time histories of the measured temperatures of the inner surface of the Inconel skin of the test nose are presented in figure 8. As previously mentioned, commutation of the thermocouple pickups stopped during firing of the second-stage motor and, hence, temperature data were not obtained during the accelerating portion of flight. The data were obtained starting at about 6.7 seconds when the model began decelerating and primarily represent the case where the recovery temperature was lower than the skin temperature or the case for heat flow from the skin to the stream. Figure 8(a) presents the six temperature measurements along the one meridian of the 100° cone portion of the test nose. In order to facilitate presentation of these data, staggered scales have been used in this figure. The measurements at thermocouple 3 are not consistent with the other temperature data; however, there was no evidence that this thermocouple malfunctioned during the flight. The three temperature measurements on the 10° half-angle flare of the test nose, which were taken along the same meridian as those for the previous cone temperatures, are presented in figure 8(b). In figure 8(c) there are presented the measured temperatures at stations 11 and 12 along with a repeat of the data measured at station 4. All three of these measurements are at the same longitudinal station but displaced radially around the nose cone. Except for deviations at the time between 7 and 7.6 seconds, these data show very good agreement.

Cross plots of the data of figures 8(a) and 8(b) for the arbitrarily chosen times of 6.9, 8.1, and 10 seconds are presented in figure 9. The temperatures at the stagnation point have been omitted since the nose-piece was several times thicker than the skin of the nose cone. The curve for $t = 6.9$ seconds indicated that prior to this time the heating on the 100° cone portion of the test nose probably was of a laminar level up to about 3.5 inches from the nose tip and that turbulent heating

probably existed on the rear portion of the cone. The temperature just to the rear of the cone-flare junction is considerably lower than the rearward flare temperatures and very much lower than the cone temperatures just ahead of the juncture. These lower temperatures are apparently due to the rapid expansion of the flow around the juncture. Recent heat-transfer measurements made on a flat-faced conical nose shape reported in reference 6 showed a very similar trend in the heating just to the rear of the juncture of the flat face with the conical portion of the nose.

Figure 10 presents the variation of measured Stanton number with longitudinal distance for the arbitrarily chosen times of 7.0, 8.0, 9.0, 10.0, and 12.0 seconds. Stagnation-point values have been omitted because of the uncertainty of the gradient in the thick nose piece. In the reduction of the data to Stanton numbers, radiation and conduction effects were neglected. Calculations indicated that radiation and conduction along the skin were negligible for the test conditions. The lower solid-line curves were calculated by using flat-plate laminar theory (ref. 7) corrected for conical flow as indicated in reference 8. The upper solid-line curves were calculated from the theoretical turbulent flat-plate skin-friction coefficients (refs. 9 and 10) adjusted for conical flow as noted in reference 8 and using a value of 0.6 for the ratio of Stanton number to skin-friction coefficient. Local flow conditions for the calculations were determined by using the measured surface static pressures in conjunction with theoretical conical flow values obtained from reference 11.

Although the data of figure 10 have a large amount of scatter, it should be noted that, almost without exception, all the Stanton numbers can be appreciably changed in numerical value by very small errors in the measurement of either the time rate of change of wall temperature or the temperature potential. In addition, recent tests in the radiant furnace with balsa-backed Inconel specimens, made up similar to the nose-cone construction, and with unbacked Inconel specimens that were tested at heating rates comparable with those encountered by the flight model indicated that the balsa-backing material can absorb as much as 15 percent of the total heat input. The accumulative effect of these errors is not known for certain; however, past experience indicated that trends exhibited by the data are reasonably accurate. Assuming that such is the case for the data of figure 10, it appears that transition occurred somewhere between stations at 3.0 inches and 4.5 inches at $t = 7.0$, 8.0, and 9.0 seconds. The local Reynolds numbers, based on momentum thickness, corresponding to these times and distances range from 530 to 940. These values are compatible with the results of reference 4, where values of R_{θ} ranging from 800 to 1,400 were obtained on a highly polished hemisphere-cone flight model. For $t = 10$ and 12 seconds, comparison of the data with both the laminar-flow and turbulent-flow theory

indicates that the data are transitional and that there is no definite indication of turbulent flow. In view of the previous statements made regarding the possible inaccuracies of the heat-transfer data, the local transition Reynolds numbers indicated herein should be regarded only as an order of magnitude rather than as precise values.

PRESSURE COEFFICIENTS

The measured pressures on both the nose cone and the conical flare section were reduced to pressure coefficients, and the data are presented as a function of Mach number in figure 11. In figure 11(a) the pressure coefficients for the three measurement stations on the nose cone are shown in three separate plots and include data for both the accelerating and coasting portions of the flight. In general, the agreement between the accelerating and coasting data is reasonably good. Examination of the data for the three stations on the cone shows a decrease in pressure with distance from the nose tip in the speed range from about a Mach number of 1.0 to 3.5; however, in the range from $M = 3.5$ to the peak speed of the test ($M = 4.08$) the trend with distance from the nose tip is not as clearly defined. At a Mach number of about 3.75, during both the accelerating and coasting portions of the flight, a rather sharp pressure change was measured at measurement station 2, indicating attachment of the shock wave to the nose cone. Reference 11 indicates a Mach number of 3.15 for the theoretical shock-attachment Mach number for a sharp 50° half-angle cone; however, because of the small tip bluntness of the flight nose, it would be expected that the shock wave would attach at a higher Mach number. Comparison of the measured pressure coefficients with the theoretical pressure coefficients for a sharp 50° half-angle cone (ref. 11) shows that at all three measurement stations the theory overestimates the cone pressure.

The pressure coefficients for the three measurement stations on the 10° half-angle conical flare following the nose cone are shown in figure 11(b). The majority of the data is for the accelerating portion of flight, with a few data points obtained during the coasting portion of flight. The data for all three stations generally tend to form a single line with only slight variation due to location on the flare. In the lower speed range the data indicate that the flow expands below atmospheric pressure in going around the sharp corner from the cone to the flare; however, as the speed is increased the expansion is diminished, and for speeds greater than $M \approx 3.0$ the pressure coefficients are at or near a value of zero.

SUMMARY OF RESULTS

A highly polished test nose having a relatively sharp-tipped 100° total-angle cone followed by a conical flare of 10° half-angle was flight tested to a peak Mach number of 4.08. Evaluation of the measured surface pressures and skin temperatures (the temperatures were obtained only for the case where the recovery temperature was less than the skin temperature) indicated the following results:

1. Heating on the forward 3.0 to 4.5 inches of the 100° cone was generally lower than that on the rearward portion.
2. Temperatures on the 10° flare were generally lower than the temperatures on the rearward portion of the 100° cone.
3. Local transition Reynolds numbers, based on calculated momentum thicknesses, ranged from 530 to 940 for the Mach number range from 2.72 to 3.75.
4. The measured 100° cone pressures were lower than the theoretical pressures for a sharp cone.
5. The pressure measurements on the 10° flare showed that at the lower supersonic speeds the flow expands below atmospheric pressure in going from the cone to the flare; however, as the speed increases the expansion diminishes, and for Mach numbers greater than 3.0 the flare pressure coefficients are at or near a value of zero.

Langley Aeronautical Laboratory,
National Advisory Committee for Aeronautics,
Langley Field, Va., July 22, 1957.

~~CONFIDENTIAL~~

REFERENCES

1. Rumsey, Charles B., and Lee, Dorothy B.: Measurements of Aerodynamic Heat Transfer and Boundary-Layer Transition on a 10° Cone in Free Flight at Supersonic Mach Numbers Up to 5.9. NACA RM L56B07, 1956.
2. Rumsey, Charles B., and Lee, Dorothy B.: Measurements of Aerodynamic Heat Transfer and Boundary-Layer Transition on a 15° Cone in Free Flight at Supersonic Mach Numbers Up to 5.2. NACA RM L56F26, 1956.
3. Bond, Aleck C., and Rumsey, Charles B.: Free-Flight Skin Temperature and Pressure Measurements on a Slightly Blunted 25° Cone-Cylinder-Flare Configuration to a Mach Number of 9.89. NACA RM L57B18, 1957.
4. Buglia, James J.: Heat Transfer and Boundary-Layer Transition on a Highly Polished Hemisphere-Cone in Free Flight at Mach Numbers Up to 3.14 and Reynolds Numbers Up to 24×10^6 . NACA RM L57D05, 1957.
5. Chauvin, Leo T., and Speegle, Katherine C.: Boundary-Layer-Transition and Heat-Transfer Measurements From Flight Tests of Blunt and Sharp 50° Cones at Mach Numbers From 1.7 to 4.7. NACA RM L57D04, 1957.
6. Carter, Howard S., and Bressette, Walter E.: Heat-Transfer and Pressure Distribution on Six Blunt Noses at a Mach Number of 2. NACA RM L57C18, 1957.
7. Van Driest, E. R.: Investigation of Laminar Boundary Layer in Compressible Fluids Using the Crocco Method. NACA TN 2597, 1952.
8. Van Driest, E. R.: The Problem of Aerodynamic Heating. Aero. Eng. Rev., vol. 15, no. 10, Oct. 1956, pp. 26-41.
9. Van Driest, E. R.: The Turbulent Boundary Layer for Compressible Fluids on a Flat Plate With Heat Transfer. Rep. No. AL-997, North American Aviation, Inc., Jan. 27, 1950.
10. Van Driest, E. R.: The Turbulent Boundary Layer With Variable Prandtl Number. Rep. No. AL-1914, North American Aviation, Inc., Apr. 2, 1954.
11. Ames Research Staff: Equations, Tables, and Charts for Compressible Flow. NACA Rep. 1135, 1953. (Supersedes NACA TN 1428.)

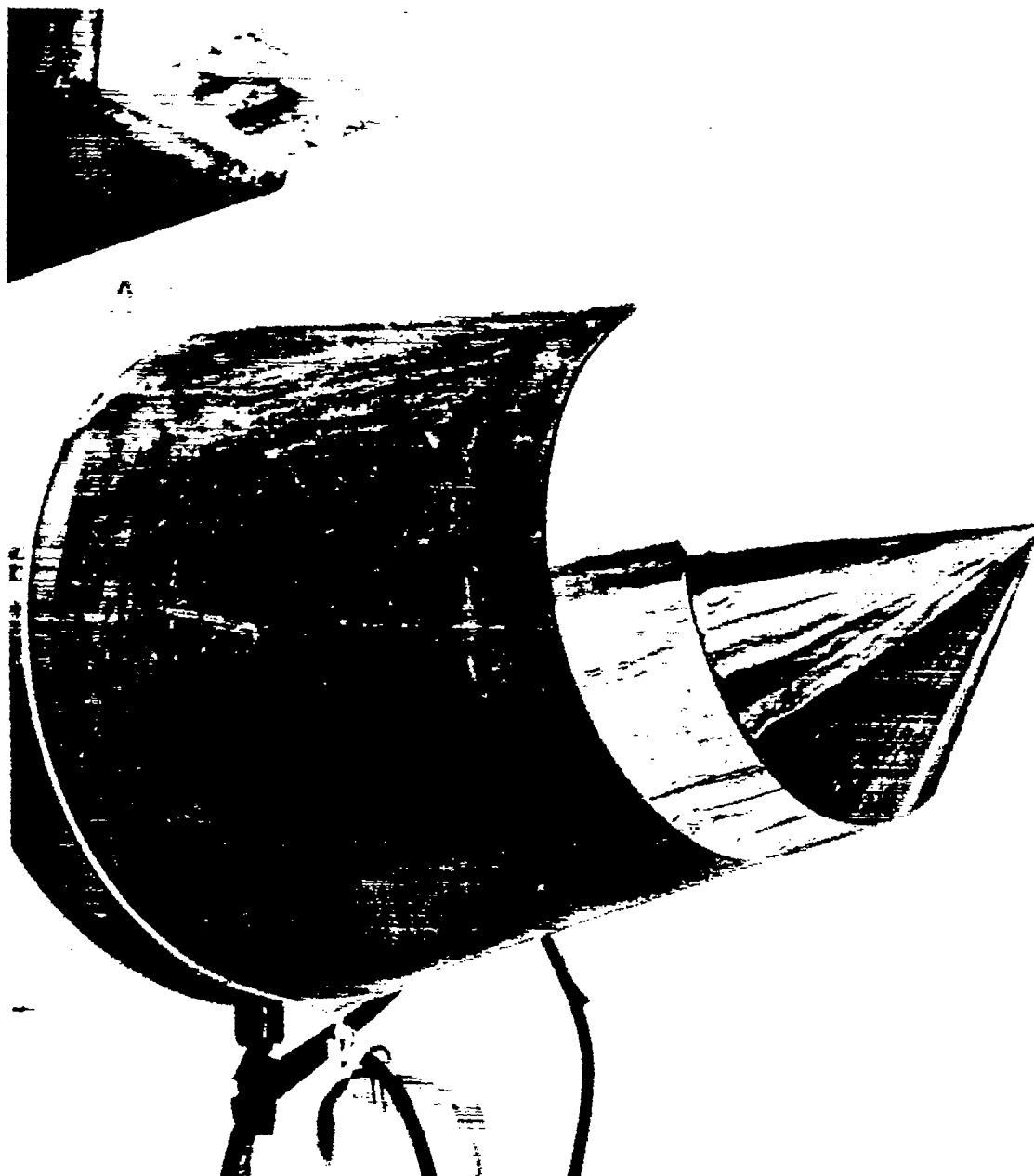
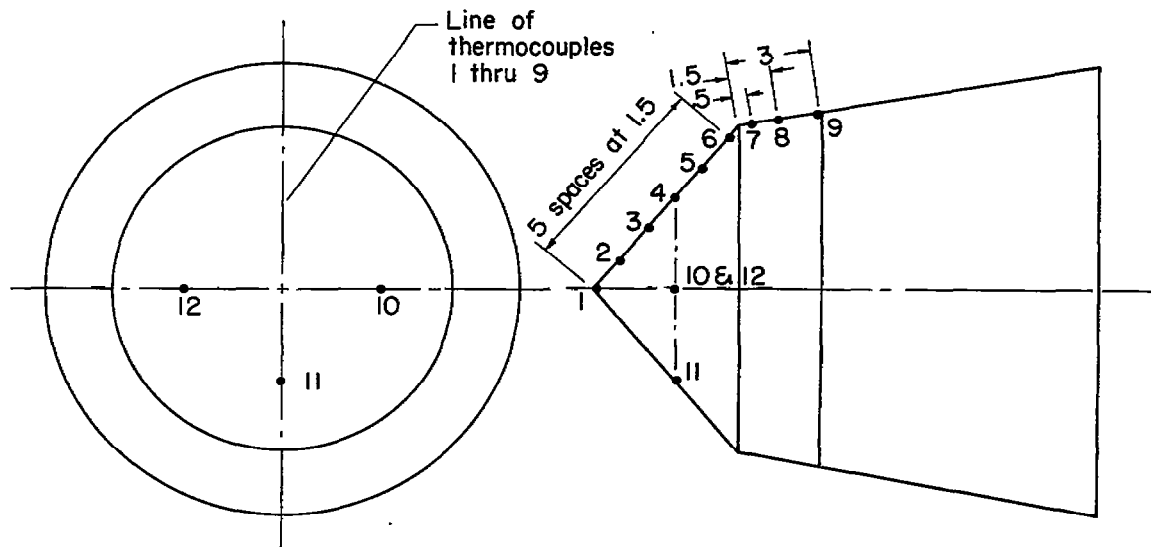
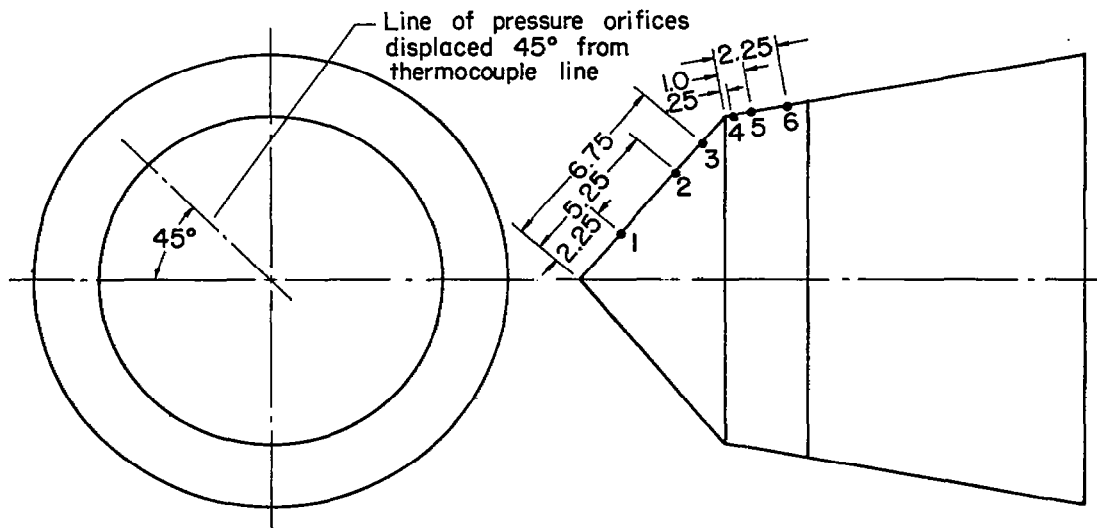


Figure 2.- Photograph of test nose.

L-57-366



(a) Location of thermocouples.



(b) Location of pressure orifices.

Figure 3.- Location of thermocouples and pressure orifices on test nose.
All dimensions are in inches.

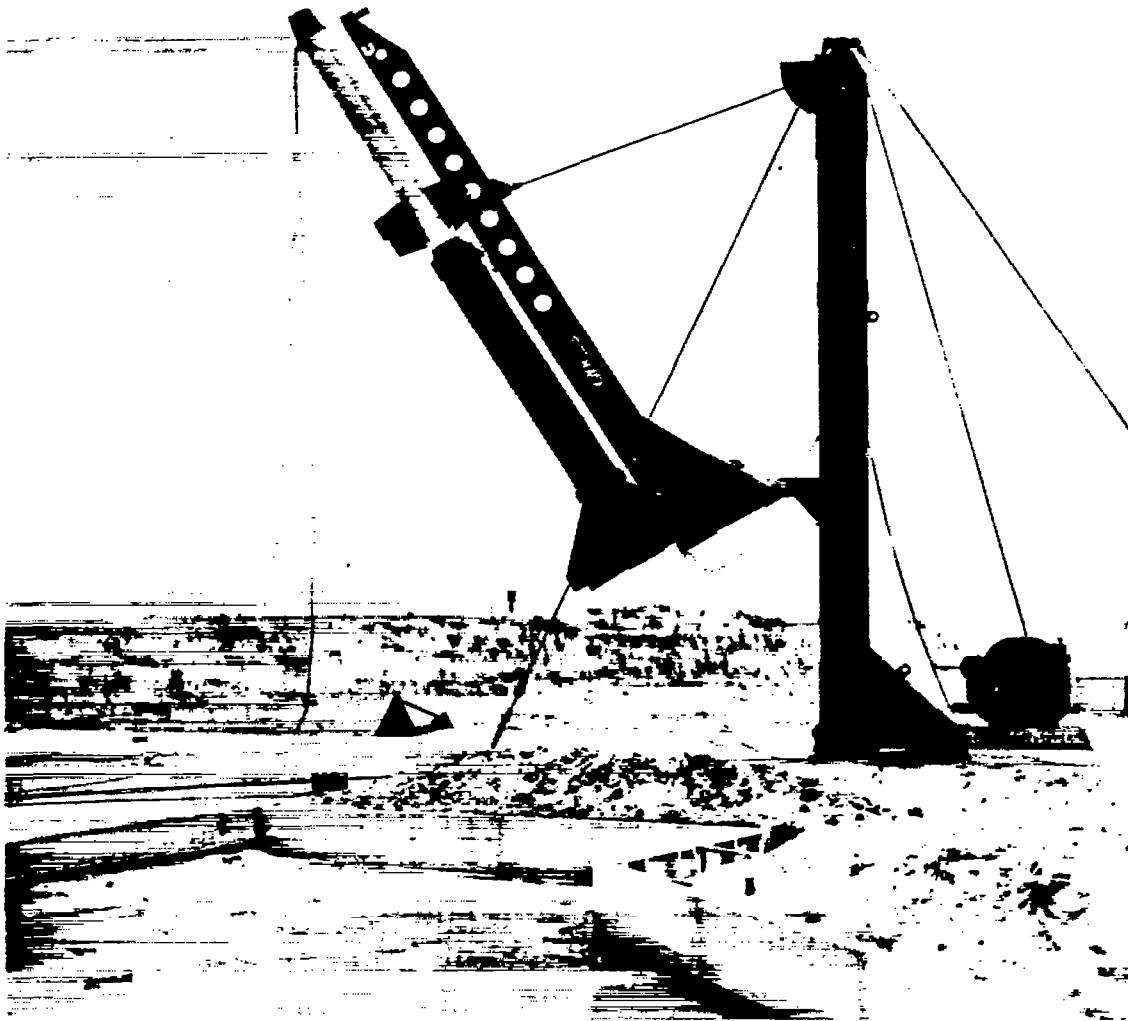


Figure 4.- Model and boosters on launcher.

L-57-368

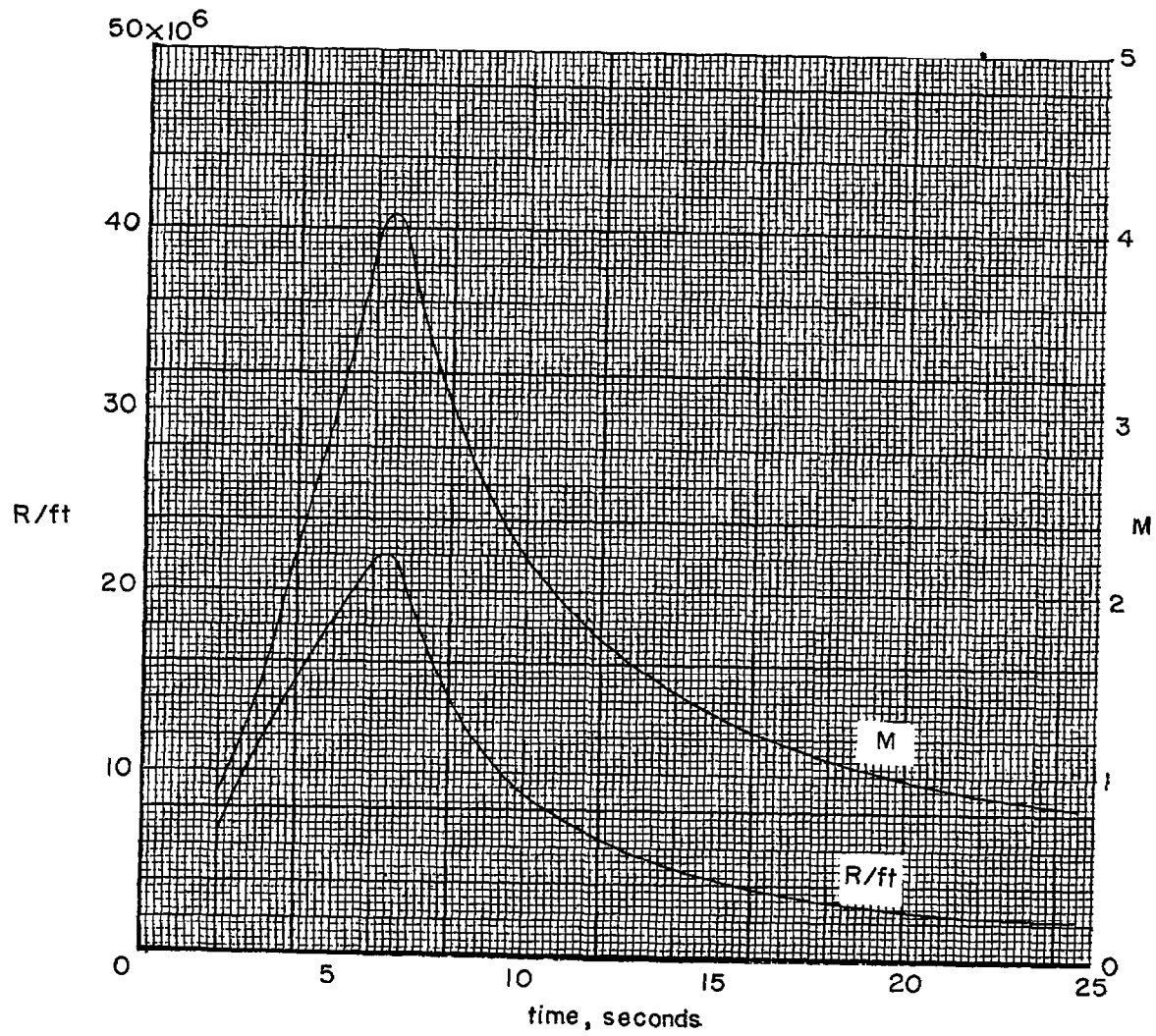


Figure 5.- Flight Mach number and free-stream Reynolds number per foot.

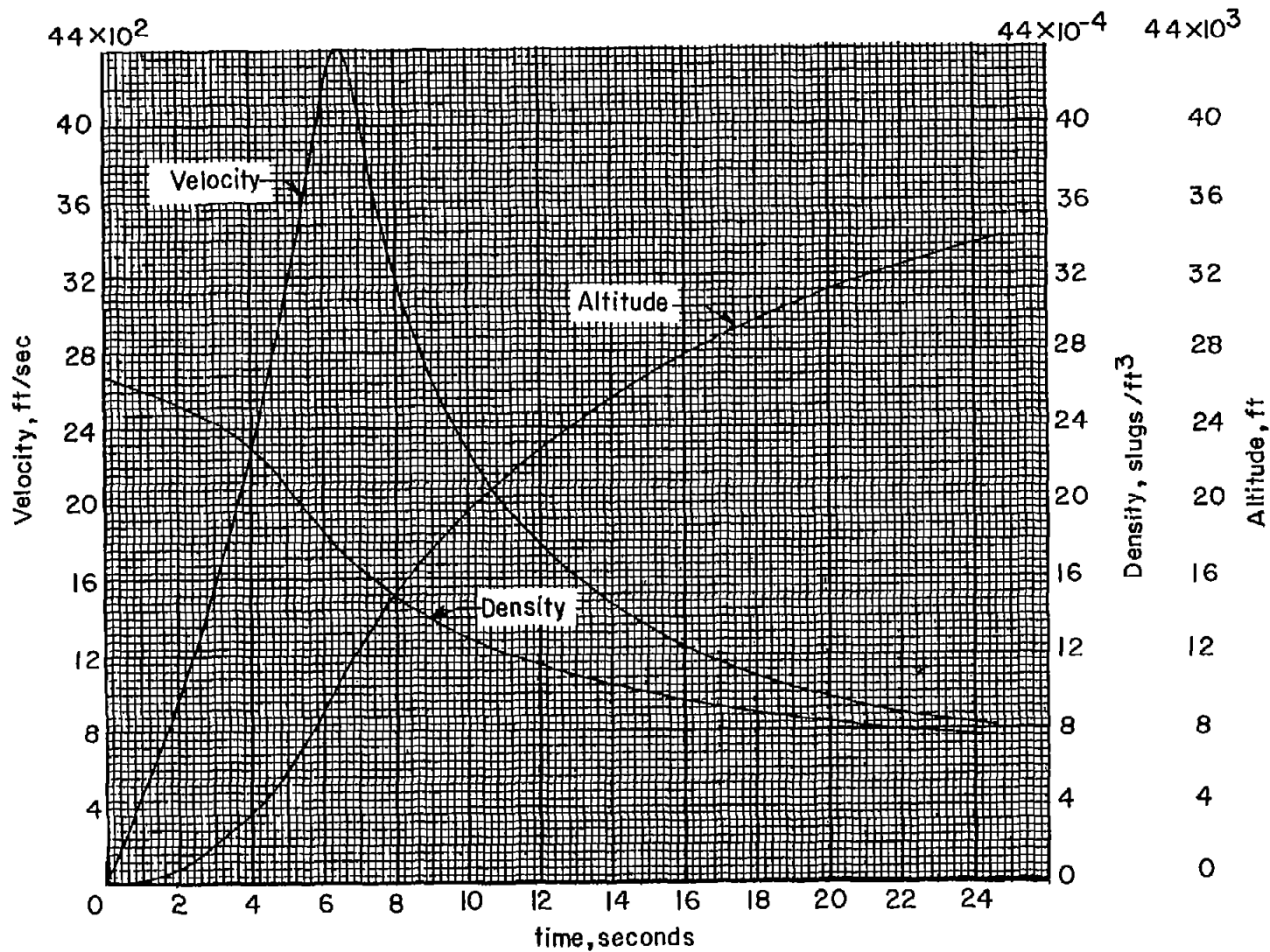


Figure 6.- Altitude, flight velocity, and free-stream density.

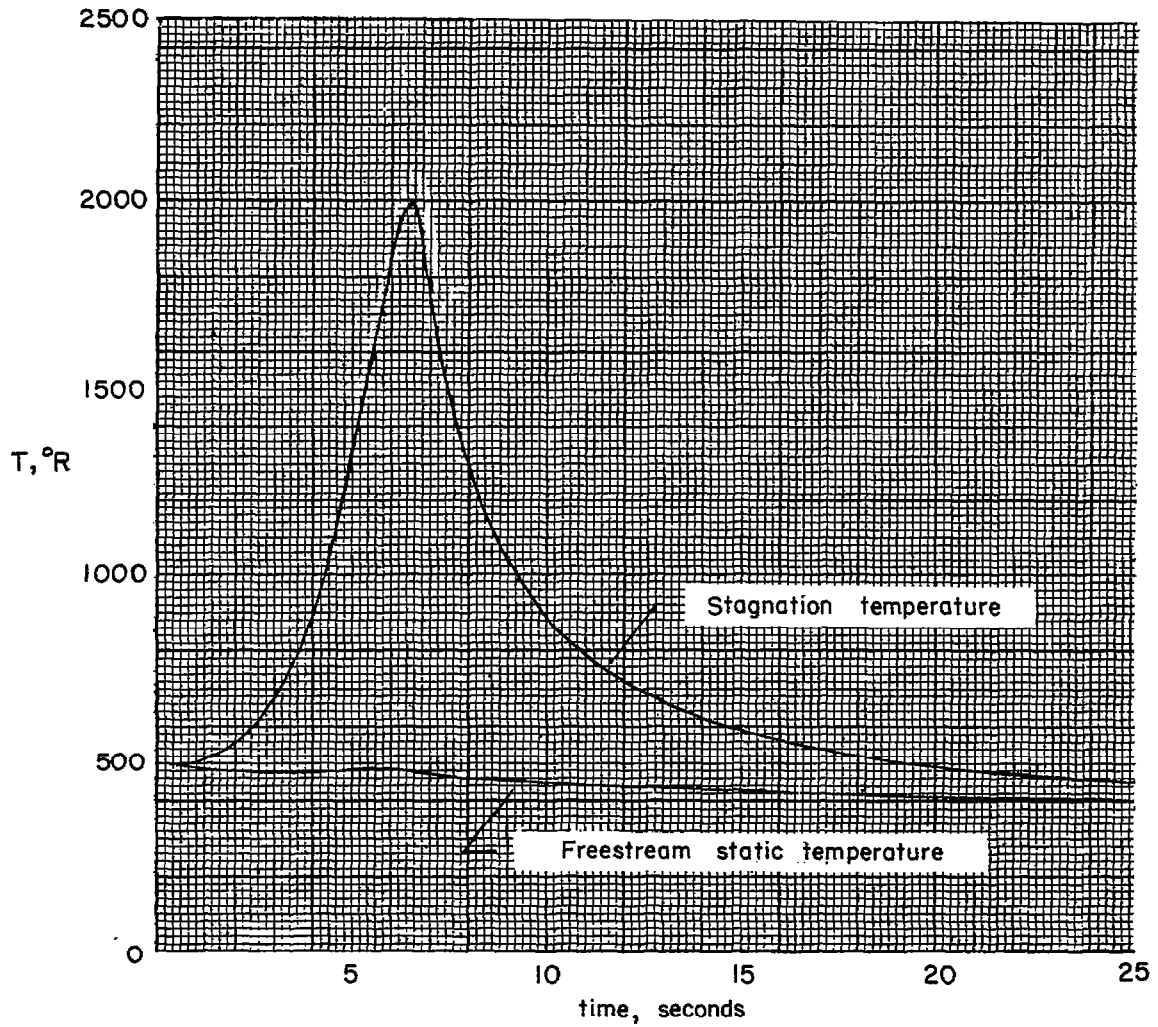
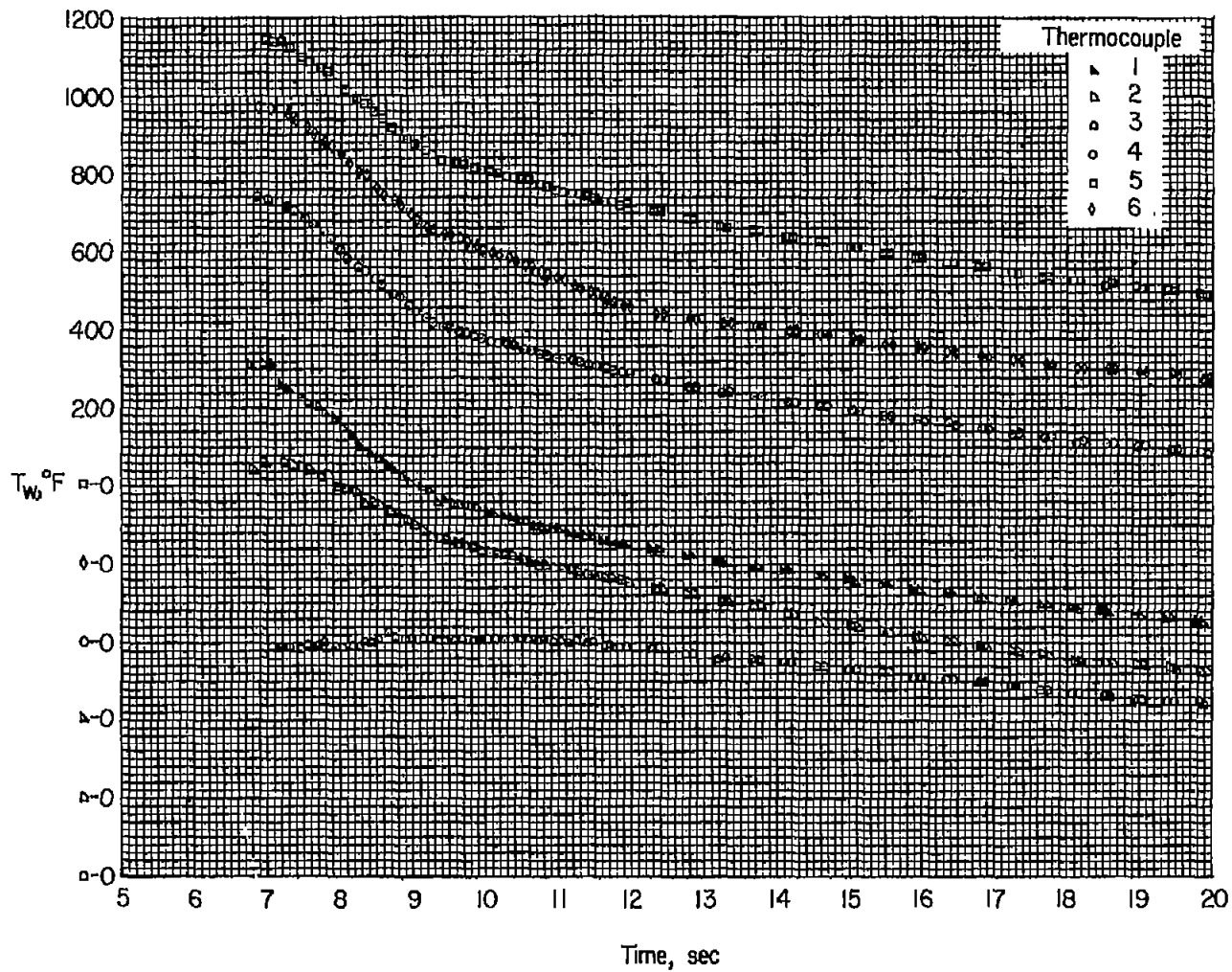
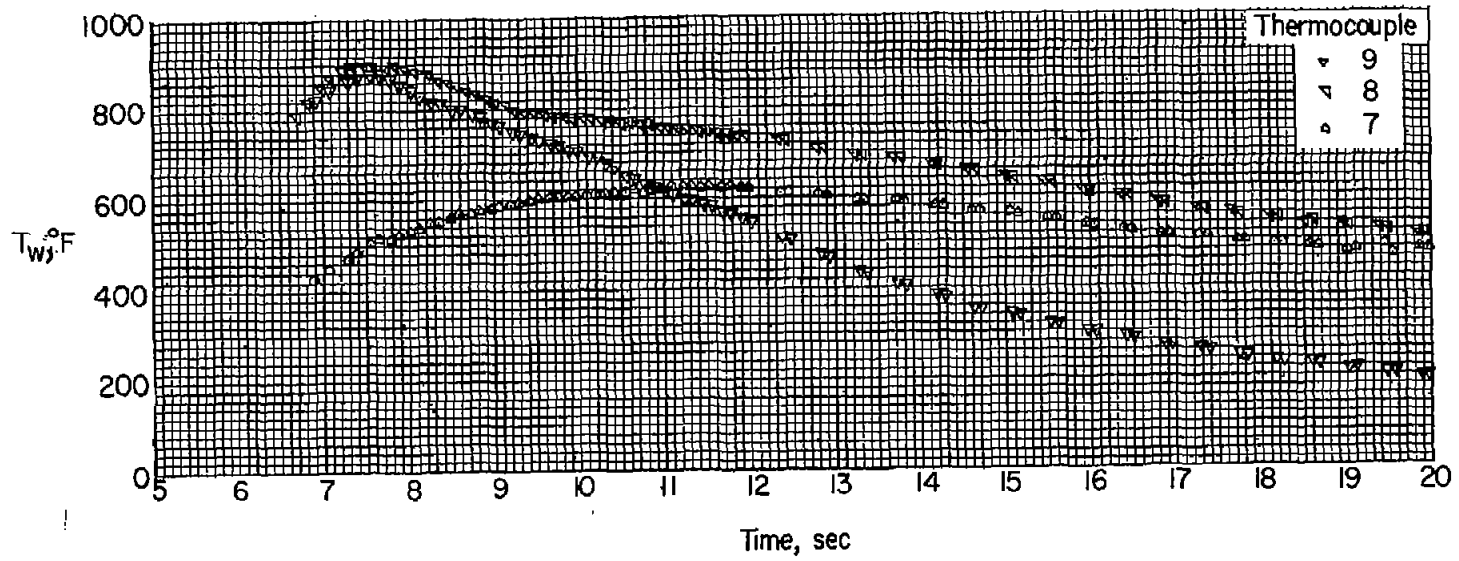


Figure 7.- Time histories of stagnation and free-stream temperatures.



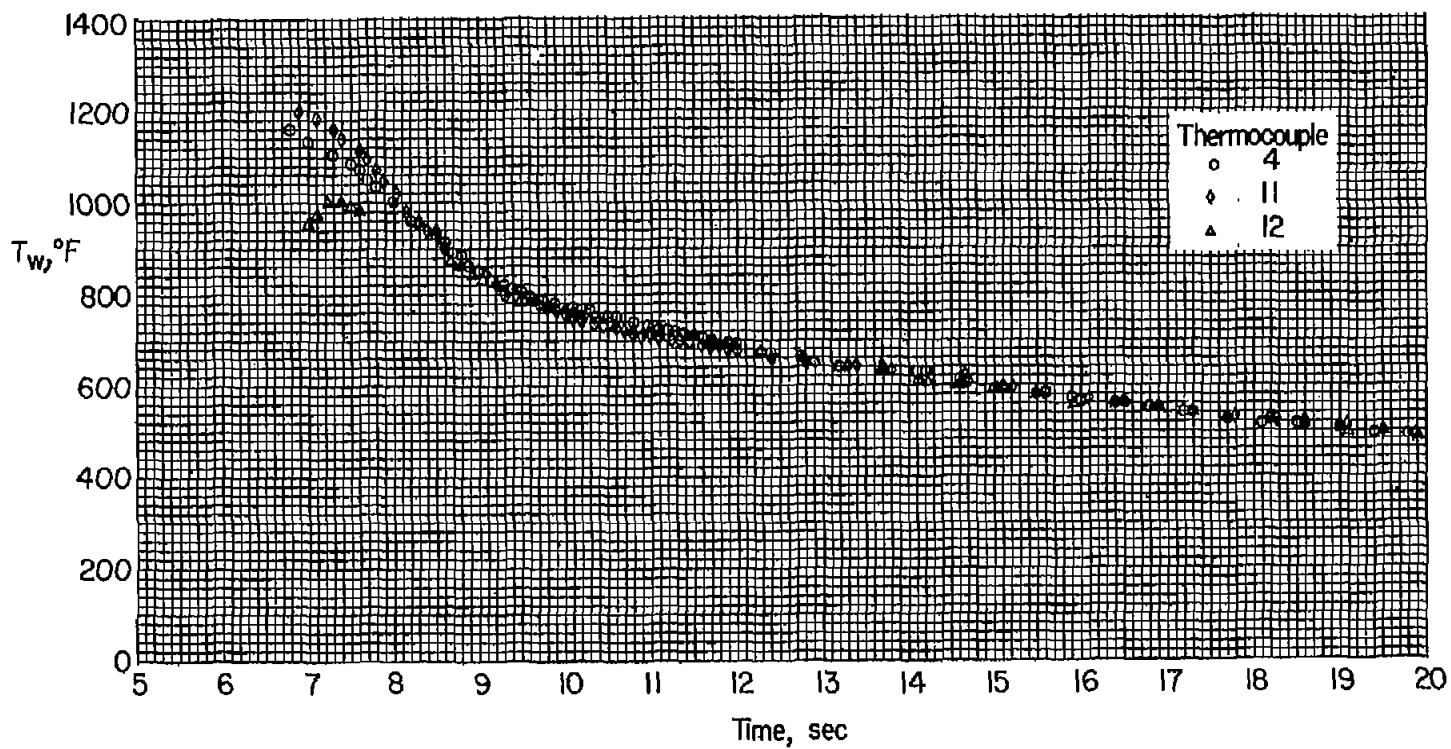
(a) Line of thermocouples on 100° cone.

Figure 8.- Time histories of skin temperatures measured on test nose.



(b) Thermocouples on 10° half-angle flare.

Figure 8.- Continued.



(c) Thermocouples at same longitudinal station on 100° cone.

Figure 8.- Concluded.

CONFIDENTIAL

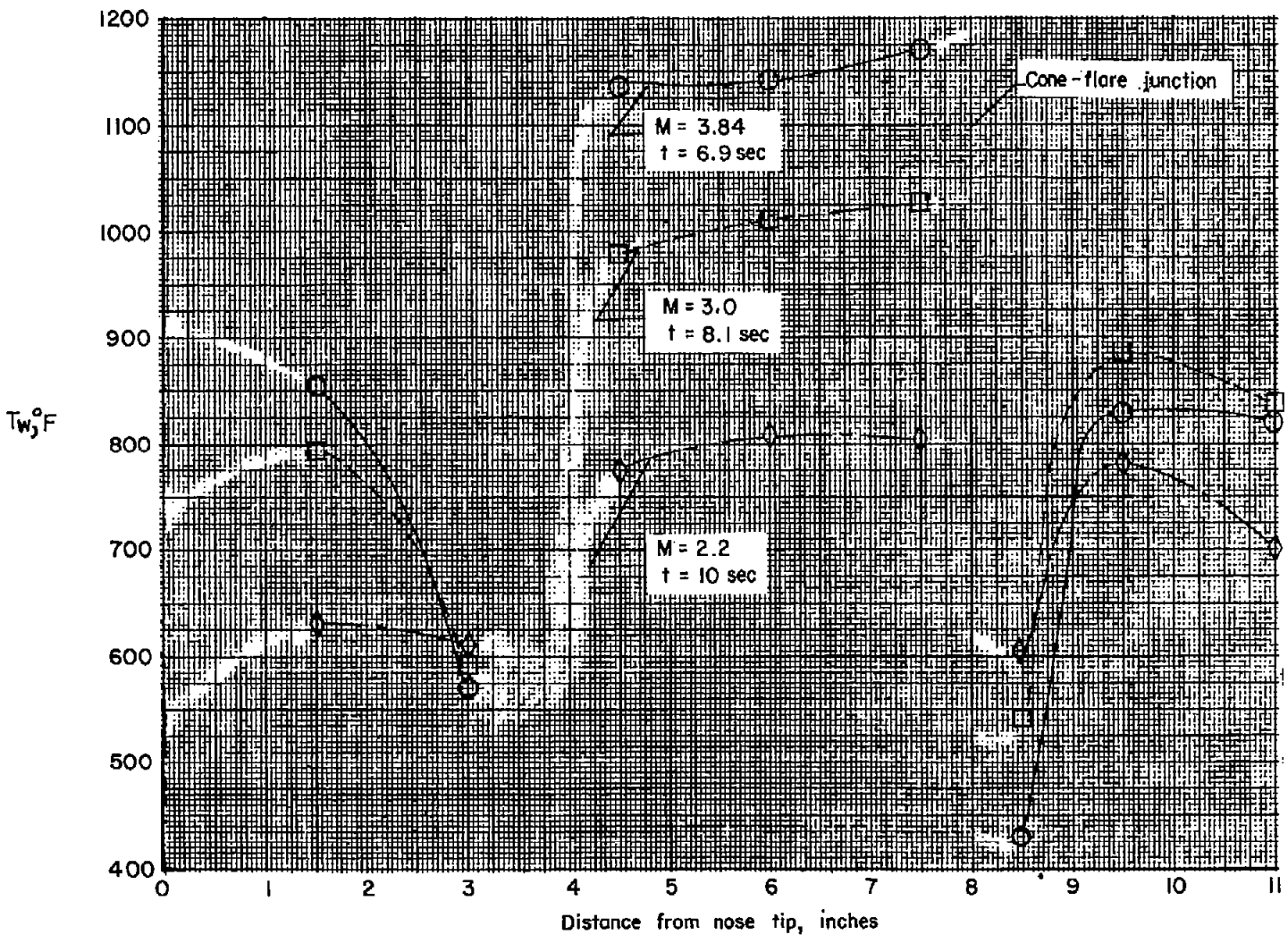
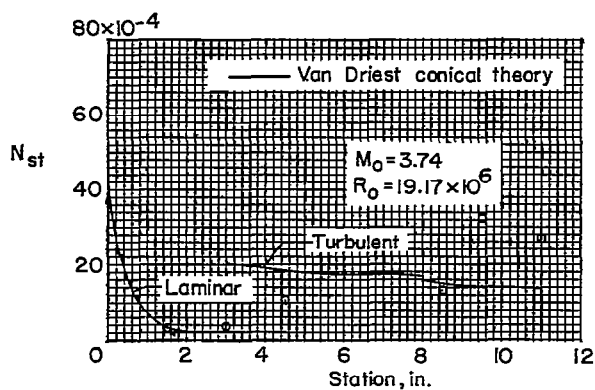
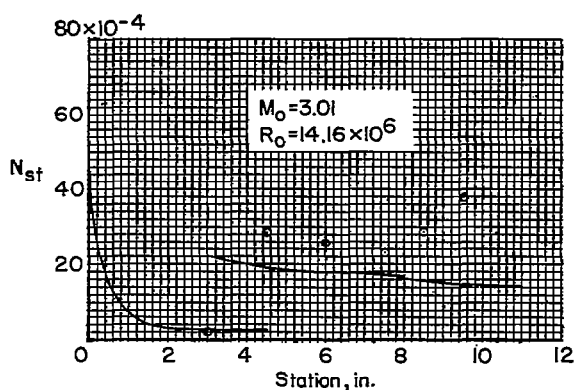


Figure 9.- Temperature distributions on test nose at various times of flight.

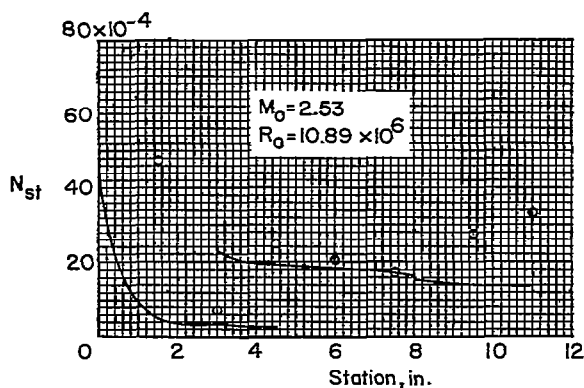
CONFIDENTIAL



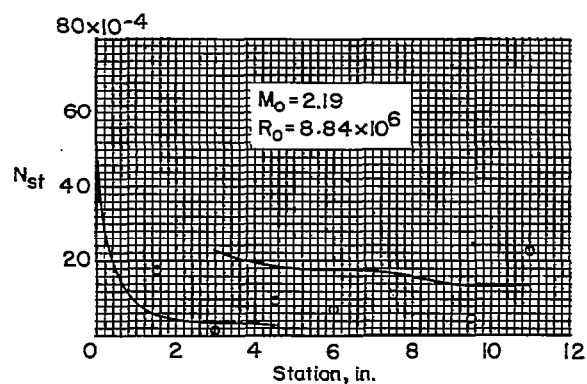
(a) 7.0 seconds.



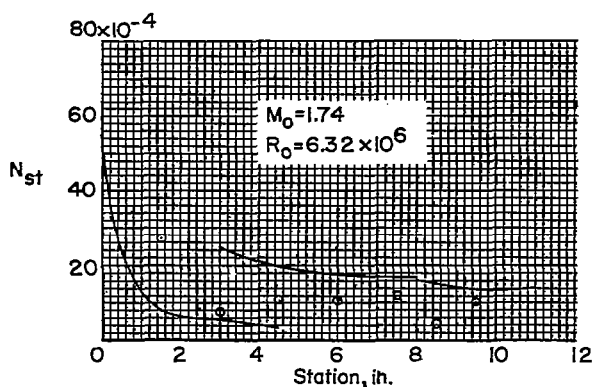
(b) 8.0 seconds.



(c) 9.0 seconds.

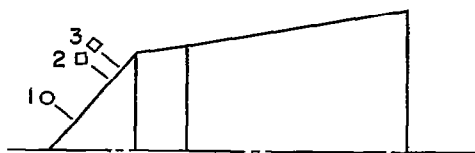


(d) 10.0 seconds.

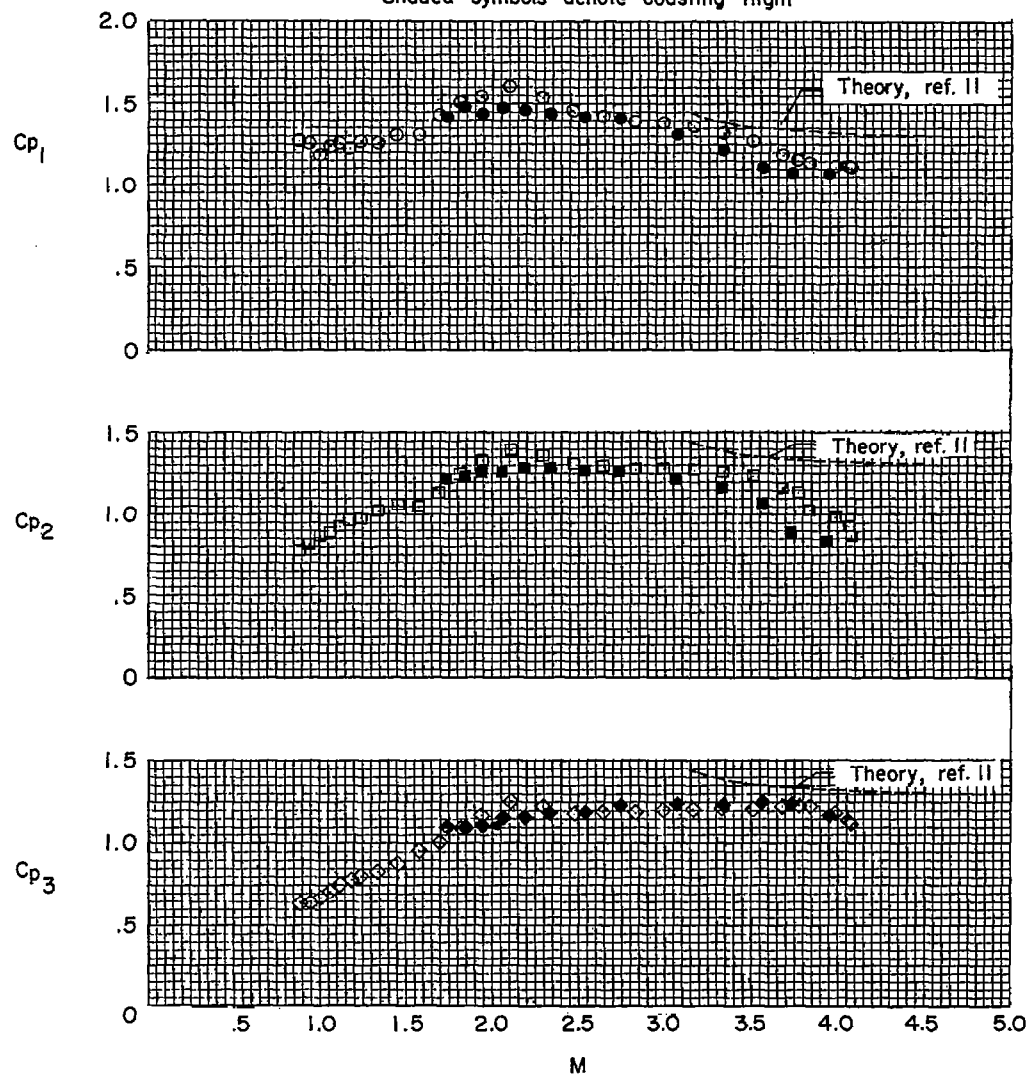


(e) 12.0 seconds.

Figure 10.- Stanton number distribution along test nose for various times during test.

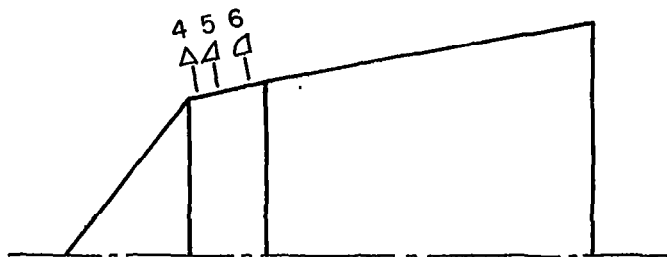


Open symbols denote accelerating flight
 Shaded symbols denote coasting flight

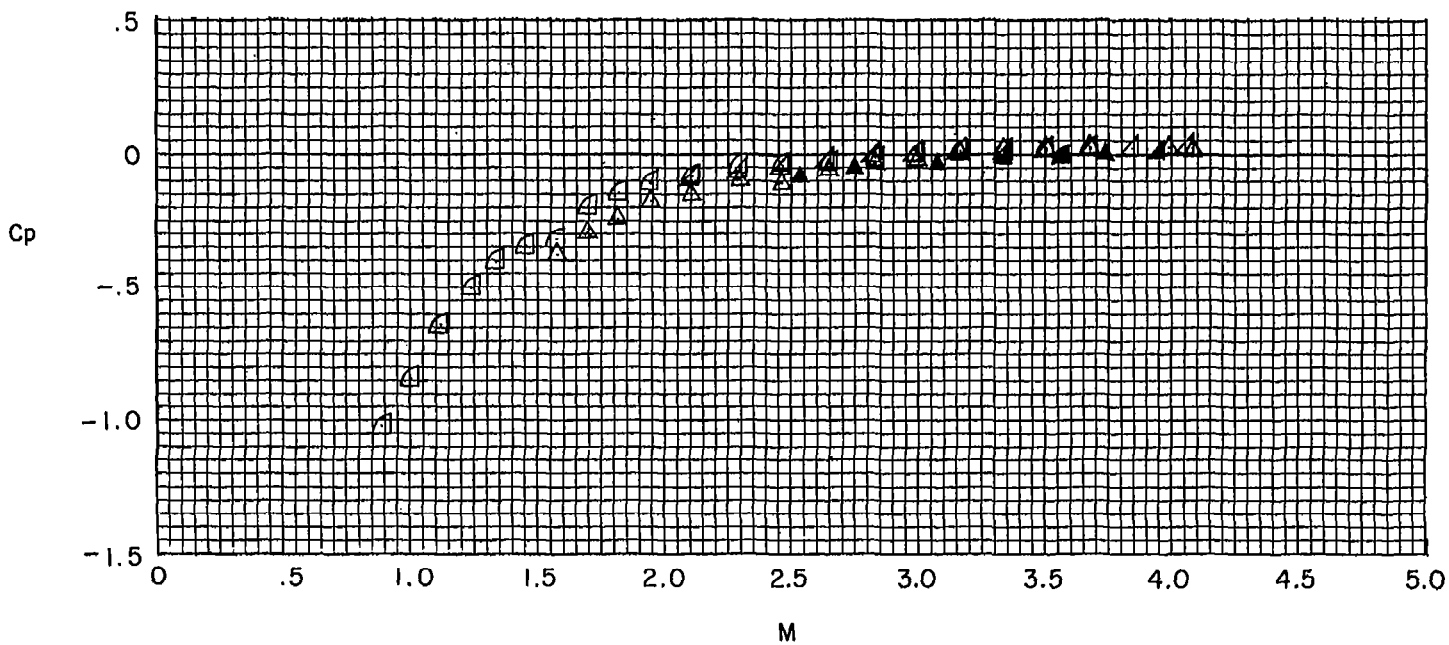


(a) Cone stations.

Figure 11.- Variation of pressure coefficients with Mach number for test nose.



Open symbols denote accelerating flight
 Shaded symbols denote coasting flight



(b) Flare stations.

Figure 11.- Concluded.

CONFIDENTIAL

CONFIDENTIAL